Primary Malignant Rhabdoid Tumor of the Brain: Clinical, Imaging, and Pathologic Findings

Soheil L. Hanna,[1] James W. Langston,[1,4] David M. Parham,[2] and Edwin C. Douglass[3]

PURPOSE: To describe the imaging and pathologic findings of malignant rhabdoid tumor (MRT), a rare primary brain neoplasm affecting children. **METHODS:** The CT and/or MR features, pathologic findings, and clinical records of three children with primary MRT of the brain were retrospectively reviewed. **RESULTS:** The tumors, large, left-sided cerebral masses, were intraventricular in two cases. MR images in one patient showed T1- and T2-weighted signal intensity isointense with gray matter. Multiple necrotic/cystic foci were present in all cases, with two showing a patchy pattern of enhancement on CT and MR. The diagnosis of MRT was documented by ultrastructural and immunohistochemical studies. All patients had normal abdominal CT scans, excluding the possibility of primary renal rhabdoid tumor metastatic to the brain. The disease progressed rapidly in each case, despite surgery, chemotherapy, and craniospinal irradiation, with serial imaging evidence of tumor regrowth at the primary site and the development of metastatic satellite lesions. **CONCLUSIONS:** The diagnosis of primary MRT of the brain can be made only pathologically; however, the nonspecific imaging findings in these cases suggest that MRT should be considered in the differential diagnosis of large childhood intracranial neoplasms.

Index terms: Brain neoplasms, in infants and children; Sarcoma; Pediatric neuroradiology

AJNR 14:107–115, Jan/Feb 1993

Malignant rhabdoid tumor (MRT) is an uncommon childhood neoplasm that typically arises within the kidney. It is characterized by an aggressive clinical course. Since its recognition in 1978 (1), six cases of primary intracranial MRT have been reported (2–7). Only two of these included a description of the imaging findings (6, 7). This report presents three additional cases with their clinical, imaging, and pathologic findings.

Received December 12, 1991; revision requested January 27, 1992; revision received February 21 and accepted March 18.

Supported in part by the National Cancer Institute, Cancer Center Support (CORE) Grant P30CA21765 and CA23099 and by the American Lebanese Syrian Associated Charities.

[1] Department of Diagnostic Imaging, St. Jude Children's Research Hospital, Memphis, TN, and Department of Radiology, University of Tennessee, Memphis, TN.

[2] Department of Pathology and Laboratory Medicine, St. Jude Children's Research Hospital, Memphis, TN, and Department of Pathology, University of Tennessee, Memphis, TN.

[3] Department of Hematology-Oncology, St. Jude Children's Research Hospital, Memphis, TN, and Department of Pediatrics, University of Tennessee, Memphis, TN.

[4] Address correspondence and reprint request to Dr James W. Langston, Department of Diagnostic Imaging, St. Jude Children's Research Hospital, PO Box 318, 332 N Lauderdale, Memphis, TN 38101-0318.

AJNR 14:107–115, Jan/Feb 1993 0195-6108/93/1401-0107

Materials and Methods

Clinical Findings

We reviewed the clinical, imaging, and pathologic features of three patients with primary MRT of the brain, one boy and two girls, aged 8, 25, and 66 months at the time of presentation. The diagnosis of MRT was established by light and electron microscopy and immunohistochemistry following partial or total tumor resection.

Imaging Findings

CT brain scans before and after intravenous contrast enhancement were obtained preoperatively in two patients. The third patient underwent magnetic resonance (MR) imaging. All patients also underwent contrast-enhanced computed tomography (CT) scans of the abdomen at the time of diagnosis to exclude primary renal tumors. Postoperative follow-up brain imaging was routinely performed using CT or MR to assess the effects of chemotherapy and craniospinal irradiation.

TABLE 1: Summary of clinical findings in patients with primary malignant rhabdoid tumor of the brain

Case No.	Age (yr)	Sex	Symptoms	Treatment	Outcome	Autopsy
Our series						
1	2	F	Lethargy, ataxia, disconjugate vision, fever, and vomiting	Partial resection; chemotherapy,[a] craniospinal RT (4950 cGy)[b]	Died 6 months postoperatively	Not performed
2	0.6	M	Lethargy, increased irritability, right extremity tremors, and vomiting	Total resection; chemotherapy,[c] craniospinal RT (5000 cGy)[b]	Died 15 months postoperatively	Not performed
3	5.5	F	Diplopia and fatigue	Total resection; chemotherapy,[d] craniospinal RT (6255 cGy)[b]	Died 6 months postoperatively	Not performed
Cases reported in the literature						
Sotelo-Avila et al (2), 1986	13.3	M	Headache, tonic-clonic seizures	Partial resection; RT (3,780 cGy)	Died 3 months postoperatively	Not performed
Briner et al (3), 1985	0.2	M		Partial resection	Died 2.5 months postoperatively	Frontal meningeal metastases
Kapur et al (4), 1986	5.8	M				
Biggs et al (5), 1987	0.1	M	Apathy, hypotonia, hyperirritability, increased head size, and seizures	No treatment	Died 0.5 months following presentation	Tumor extension throughout subarachnoid space with invasion of frontal lobes
Jakate et al (6), 1988	3	F	Lethargy, neck pain, morning vomiting, and squint	Partial resection; chemotherapy; craniospinal RT	Alive 5 months postoperatively; no further followup	
Ho et al (7), 1990	4	M	Headache, poor appetite, and drowsiness	Partial resection; RT (1,340 cGy)	Died 1 month postoperatively	Not performed

Note.—RT = radiation therapy.

[a] Intrathecal methotrexate, intravenous nitrogen mustard and vincristine.

[b] Doses are total irradiation delivered to primary tumor area.

[c] Cyclophosphamide, vincristine, cisplatin, and etoposide.

[d] Ifosfamide, etoposide, and carboplatin.

Pathology

Formalin-fixed tissue in paraffin blocks was available in all three tumors. The avidin-biotin-complex (ABC) peroxidase-complex procedure was applied to sections from each tumor, using antibodies including monoclonal antivimentin (VIM), anticytokeratin (CK), antiLeu-7 (LEU), antiepithelial membrane antigen (EMA), antiglial fibrillary acidic protein (GFAP), polyclonal antineuron-specific enolase (NSE), and anti-S100 protein (S100). For negative controls, normal rabbit serum or purified mouse plasmacytoma ascites fluid was substituted for similar dilutions of polyclonal and monoclonal antisera, respectively. Sections of skin, colon carcinomas, brain, colon, and peripheral nerve were used as positive controls. All controls yielded the anticipated reactions.

Material for electron microscopic examination was available in two cases (cases 2 and 3). Preliminary sections were cut at approximately 0.4 μm and stained with toluidine blue, and representative blocks demonstrating tumor were selected. Sections of these blocks were then stained with uranyl acetate and lead citrate and examined with a transmission electron microscope.

Results

Clinical Findings

The clinical findings and postoperative courses of the three patients with MRT are summarized in Table 1. Lethargy, vomiting, and vision disturbances were the predominant presenting symptoms. All patients had large cerebral tumors, with the maximum transverse dimension ranging from 5 to 7 cm. The tumor was left-sided in each case; two tumors were intraventricular, involving the left frontal horn (case 2) and left trigone (case 3). In all three cases, the disease progressed rapidly, resulting in death within 15 months from diagnosis, despite intensive postoperative therapy including irradiation of the primary site (4950-

TABLE 2: Imaging findings of primary malignant rhabdoid tumor of the brain

Case No.	Location	Size (cm)	Unenhanced CT		MR[a]		Enhanced Pattern	Necrosis/ Cyst	Edema	Serial Postoperative CT/MR
			Density[b]	Calcification	T1W	T2W				
Our series										
1	L parietal lobe	6 × 5 × 5.5	Patchy iso-hyperdense	None	UA	UA	Patchy	Multiple (2.5 cm)[c]	Severe	Growth at primary site, new frontal satellites
2	L frontal horn (intraventricular)	7 × 5 × 6	Slightly hyperdense	Few flecks	UA	UA	Diffuse	Multiple (1.5 cm)[c]	None	Growth at primary site, new cerebellopontine satellite
3	L trigone (intraventricular)	5.5 × 5 × 5	UA	UA	Isointense	Isointense	Patchy	Multiple (1.0 cm)[c]	Moderate	Growth at primary site, new cerebellar and cerebellopontine satellites
Cases reported in the literature										
Sotelo-Avila et al (2), 1986	L temporal lobe	5 × 4								
Briner et al (3), 1985	L parietal lobe (into lateral ventricle)	Large								
Kapur et al (4), 1986	Cerebellum									
Biggs et al (5), 1987	Cerebellum	Large								
Jakate et al (6), 1988	L cerebellum (into fourth ventricle)	Large	Mixed				Intense			
Ho et al (7), 1990	Multifocal		Dense	Linear, punctate			Intense			

Note.—L = left; UA = unavailable; T1W = T1-weighted; T2W = T2-weighted.

[a] T1- and T2-weighted tumor signal characteristics compared to normal gray matter.

[b] Unenhanced CT tumor density compared to normal gray matter.

[c] Size of largest necrotic/cystic focus.

6255 cGy) and multiagent chemotherapy (see Table 1).

Imaging Findings

Imaging results are given in Table 2. The unenhanced preoperative CT scans in cases 1 and 2 showed a varying density pattern, ranging from iso- to slight hyperdensity in relation to normal gray matter (Figs. 1A and 2A). There were a few scattered flecks of calcification present in one tumor (case 2). The signal characteristics of the solid tumor component of the single case imaged by MR (case 3) paralleled those of normal gray matter on T1- and T2-weighted images (Figs. 3A and 3B).

The contrast-enhanced preoperative CT and MR scans showed a patchy pattern of enhance-

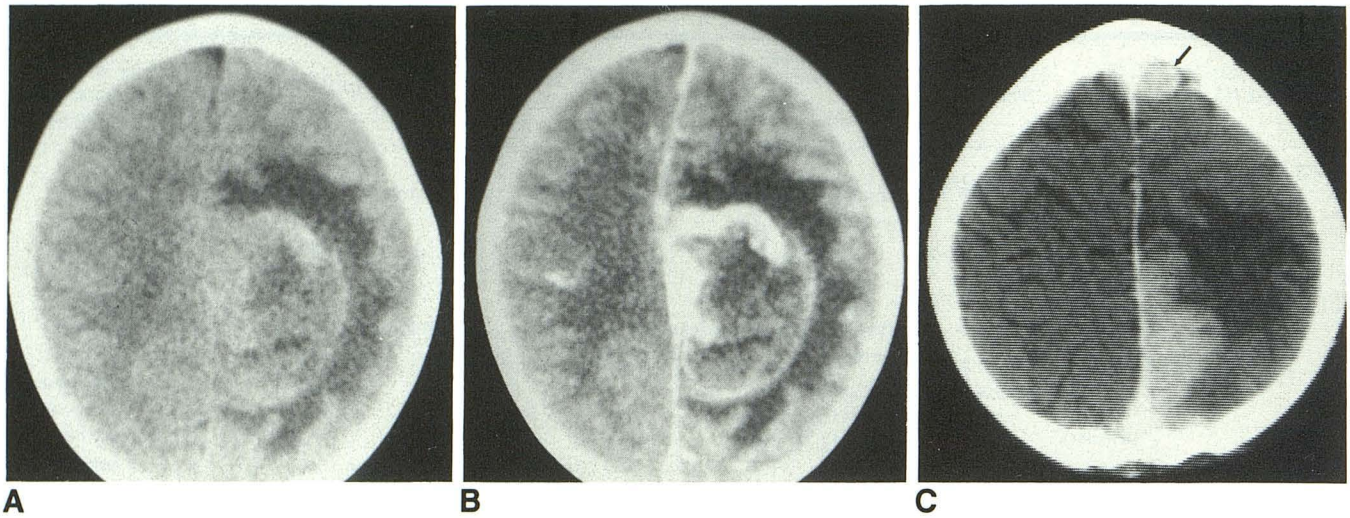

Fig. 1. Case 1: 25-month-old girl with left parietal primary MRT.

A, Unenhanced transverse CT image shows a large left supraventricular, parafalcine mass of mixed density and prominent adjacent edema.

B, Contrast-enhanced image at the same level shows intense patchy peripheral enhancement and central necrosis.

C, Postoperative contrast-enhanced CT image obtained 1-month following partial resection shows tumor regrowth about the primary site and a new frontal tumor satellite (*arrow*).

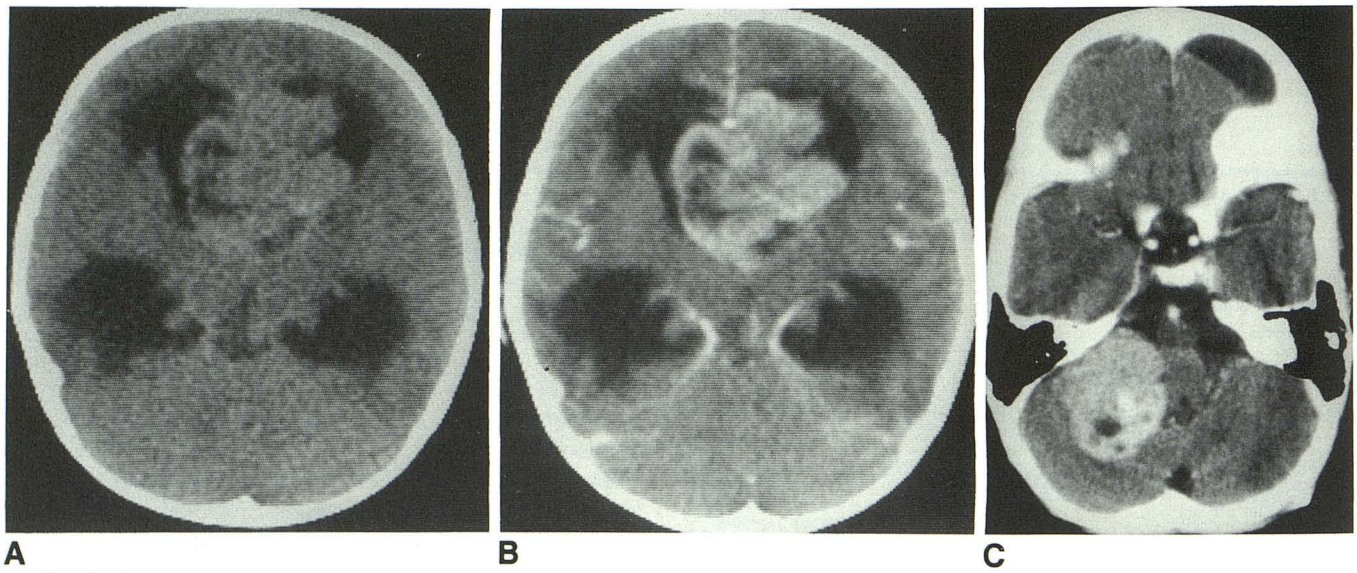

Fig. 2. Case 2: 8-month-old boy with frontal intraventricular primary MRT.

A, Unenhanced transverse CT image shows an intraventricular slightly dense tumor centered about the left frontal horn and crossing to the opposite horn.

B, Contrast-enhanced image at the same level shows intense diffuse tumor enhancement with several 1.5-cm necrotic/cystic areas.

C, Posttreatment contrast-enhanced CT image obtained 10 months later shows a large extraaxial cerebellopontine tumor satellite.

D, Electron micrograph of tumor cell demonstrating a prominent cytoplasmic inclusion composed of tightly packed whorls of intermediate filaments (*F* = filaments, *N* = nucleus; ×12,400).

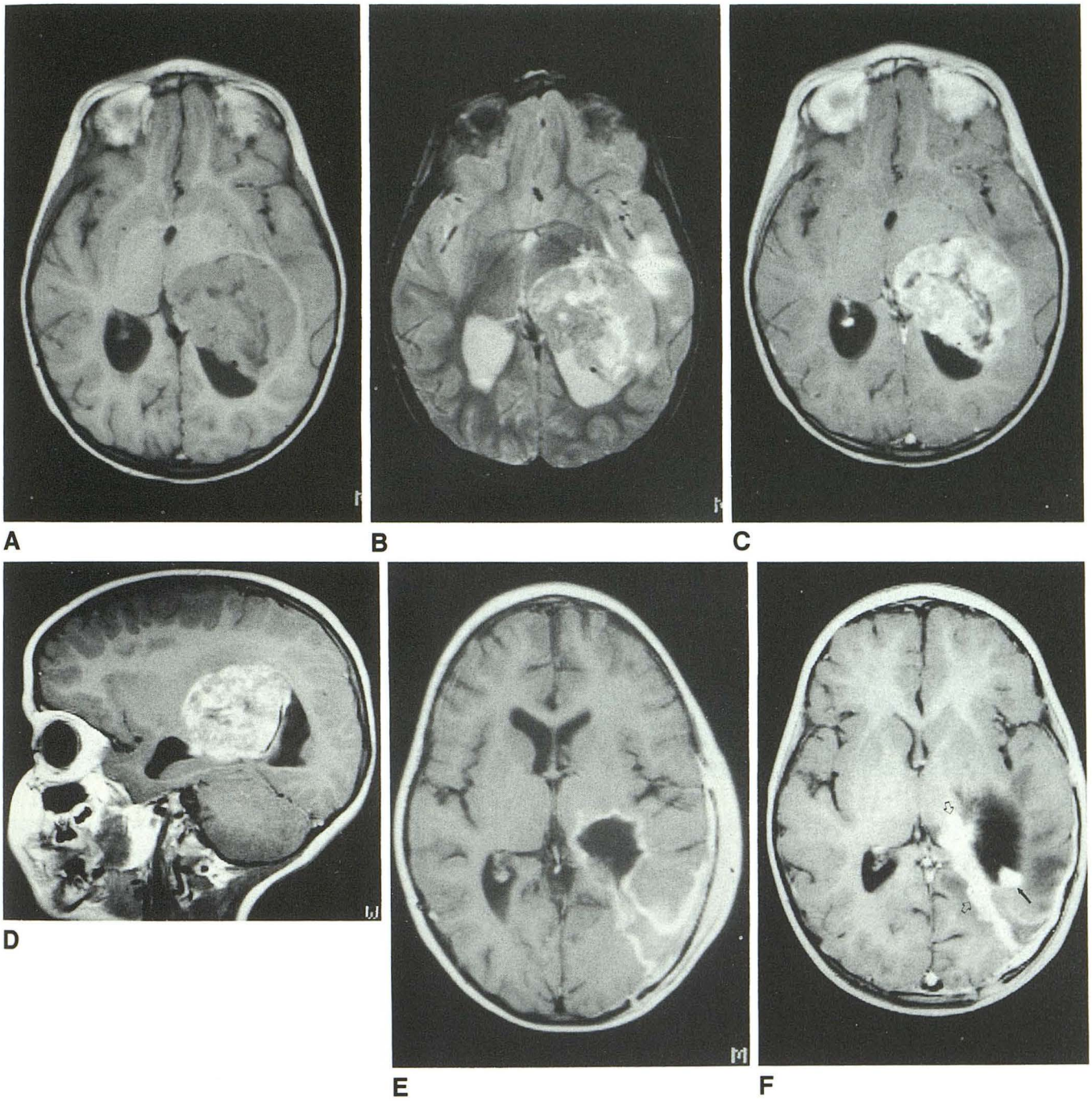

Fig. 3. Case 3: 66-month-old girl with left lateral intraventricular primary MRT.

A and *B*, Transverse T1-weighted (520/15) (*A*), and T2-weighted (2500/90) (*B*) images obtained at the same level show a large mass predominantly isointense with gray matter centered about the trigone of the left lateral ventricle. There is moderate associated parenchymal edema consistent with brain invasion.

C and *D*, Postcontrast transverse (*C*) and sagittal (*D*) T1-weighted (520/15) images show patchy tumor enhancement with small central nonenhanced necrotic areas.

E, Postcontrast transverse T1-weighted (520/15) image obtained 2 weeks after surgery shows linear enhancement about the margins of resection consistent with gliosis without evidence of residual tumor. Note also, smooth dural postoperative enhancement.

F, Transverse contrast-enhanced T1-weighted image (520/15) at the same level as *E* obtained 1.5-month later shows nodular (*solid arrow*) and thick irregular enhancement (*open arrows*) about a portion of the surgical margins consistent with tumor recurrence.

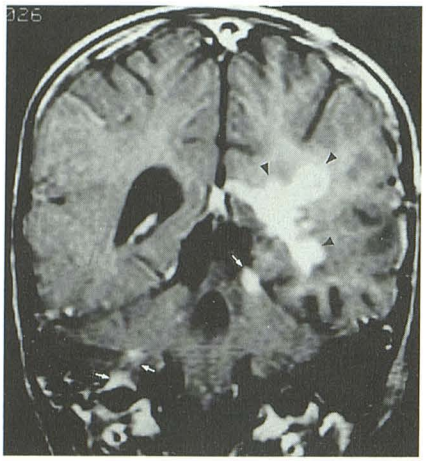

G

Fig. 3. *Continued. G*, Coronal contrast-enhanced T1-weighted image (700/30) obtained 4 months after *F* shows continued tumor growth at the primary site (*arrowheads*) and interval development of enhancing metastases (*white arrows*).

H, Photomicrograph illustrating tumor composed of diffuse sheets of cells with eccentric nuclei (*straight black arrows*), prominent nucleoli (*white arrows*), abundant cytoplasm, and discrete cytoplasmic inclusions (*curved arrows*) (hematoxylineosin, ×450).

I, Antivimentin stain illustrating strong brown (*arrows*) cytoplasmic immunoreactivity (ABC method, ×450). This correlates with the filamentous bundles detected by electron microscopy and is a characteristic feature of rhabdoid tumors at all sites.

J, Antiepithelial membrane antigen stain illustrating brown (*arrows*) membranous immunoreactivity (ABC method ×450). Epithelial membrane antigen reactivity is also a characteristic feature of rhabdoid tumors at all sites.

K, Antineuron-specific enolase stain illustrating moderate to weak brown (*arrows*) cytoplasmic immunoreactivity (ABC method, ×450). Immune reaction for this antigen may be indicative of neural differentiation or histogenesis.

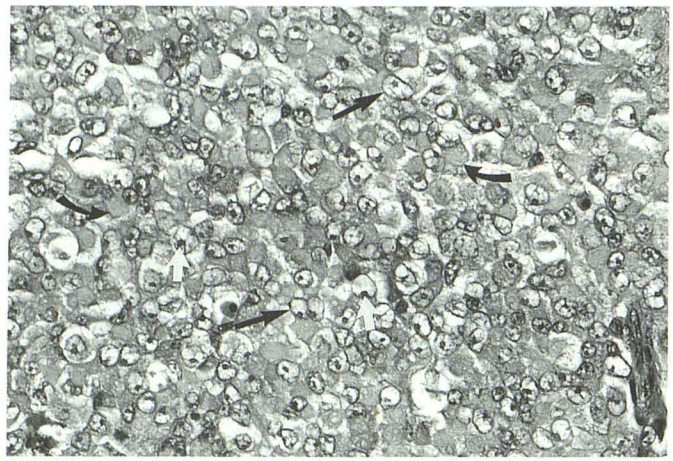

H

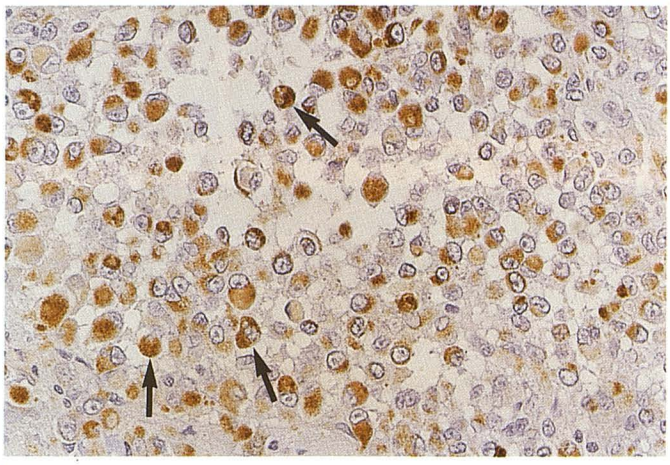

I

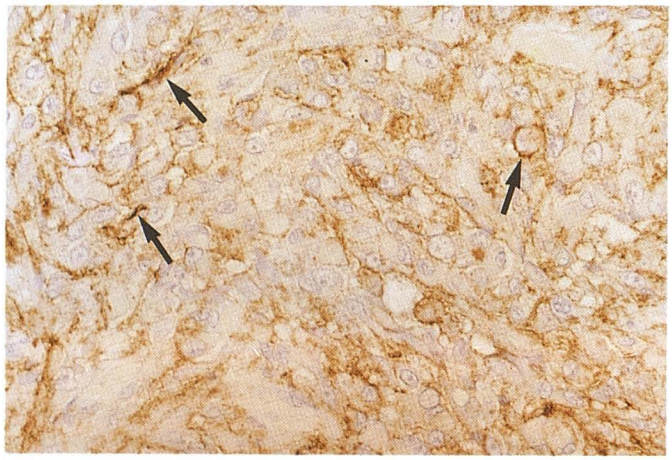

J

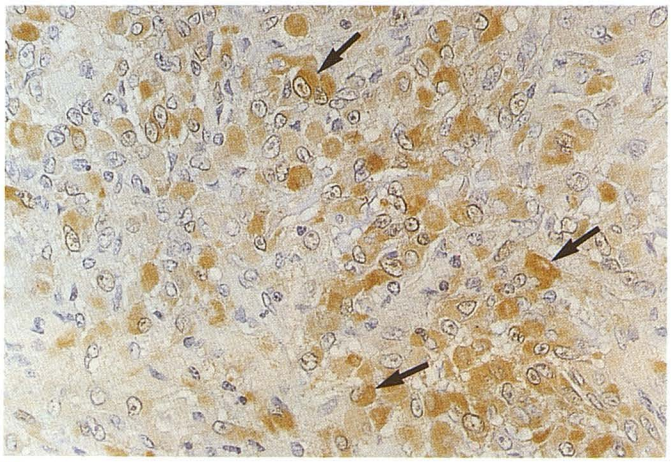

K

ment of the solid tumor component in two cases (Figs. 1B, 3C, and 3D) and a uniform pattern in one (Fig. 2B). All tumors showed multiple necrotic/cystic foci of 1.0 to 2.5 cm diameter. Images of two tumors revealed moderate to marked adjacent brain edema; the other lesion (case 2) was entirely intraventricular and caused only interstitial edema secondary to obstructive hydrocephalus (Fig. 2). Serial CT and/or MR imaging following either total or partial tumor resection indicated tumor regrowth at the primary site (Figs. 1C, 3E, and 3F) and new, rapidly

TABLE 3: Light microscopic and immunohistochemical features of primary malignant rhabdoid tumors of the brain

Case No.	Light Microscopy				Immunohistochemistry						
	N	C	I	P	VIM	CK	EMA	GFAP	NSE	LEU	S100
1	3+	3+	1+	Ep,Cl	3+	2+	2+	0	2+	0	3+
2	1+	3+	1+	Sp,Sc	3+	3+	3+	0	0	3+	2+
3	3+	3+	2+	Sp,Ep	2+	1+	2+	2+	1+	0	3+

Note.—N = typical nuclei; C = typical cytoplasm; I = cytoplasmic inclusions on routine staining; P = histologic pattern according to Weeks et al (8); Cl = classical pattern; Sp = spindled pattern; Sc = sclerosing pattern; Ep = epithelioid pattern; VIM = vimentin; CK = cytokeratin; EMA = epithelial membrane antigen; GFAP = glial fibrillary acidic protein; NSE = neuron-specific enolase; LEU = Leu-7; S100 = S100 protein; 0 = no tumor cells positive; 1+ = <10% of tumor cells positive; 2+ = 10–50% of tumor cells positive; 3+ = >50% of tumor cells positive.

growing meningeal masses consistent with metastases (Figs. 1C, 2C, and 3G).

Pathology

On routine stains, the cases contained cells with typical "rhabdoid" features, ie, eccentric nuclei, prominent "owls-eye" nucleoli, abundant brightly eosinophilic cytoplasm, and discrete cytoplasmic hyaline inclusions (Fig. 3H). Areas of "spindled" pattern were predominant in cases 2 and 3, whereas case 1 contained areas with the classic diffuse pattern (8) (see Table 3). Epithelioid areas were present in cases 1 and 3, and a minor component of sclerosis was present in case 2.

Areas of vimentin immunoreactivity were the most consistent immunohistochemical finding (Table 3), and revealed cytoplasmic inclusions not recognizable on routine stains (Fig. 3I). Cytokeratin immunoreactivity and varying degrees of membranous staining for epithelial membrane antigen (Fig. 3J) were present in all cases. Case 3 exhibited moderate cytoplasmic staining with anti-GFAP. The neural markers NSE, Leu-7, and S100 were variably present, but did not appear to follow a discernable pattern (Fig. 3K).

Electron microscopy, available in cases 2 and 3, revealed intermediate filaments within numerous cells in both cases. Case 2, in particular, had characteristic compact whorls of intermediate filaments (Fig. 2D). Cytoplasmic lipid vacuoles were present in case 2 and abundant in case 3. Cytoplasmic processes were present in both cases studied. Case 3 contained occasional aggregates of neurosecretory granules and parallel arrays of 25-nm microtubules. Both cases also contained numerous primitive intercellular junctions, especially in areas of process formation.

Discussion

MRT is a rare and extremely aggressive malignancy, originally regarded as a "rhabdomyosarcomatoid" variant of Wilms tumor associated with a poor prognosis (1). Since that early description, there have been several reports of primary extrarenal MRTs arising from a variety of sites, including the paravertebral region (9), chest wall (10), heart (11), liver (12), pelvis (13), uterus (14), vulva (15), prostate (16), soft tissues (17), and brain (2–7). Of six previously documented cases of primary MRT of the brain, imaging findings (CT) have been presented for only two (6, 7). Our series of three cases provides an opportunity to evaluate the tumor's clinical, imaging, and pathologic features.

The term "rhabdoid" was applied to these tumors because of their light microscopic resemblance to rhabdomyosarcoma. However, subsequent ultrastructural and immunohistochemical studies did not substantiate myogenous differentiation, indicating instead that MRT is a unique neoplasm of undetermined histogenesis, unrelated to either rhabdomyosarcoma or Wilms tumor (18, 19). Our cases fulfill the criteria for the diagnosis of MRT, including the presence of cytoplasmic aggregates of intermediate filaments, and keratin and vimentin immunoreactivity. Of particular interest is the finding of neural differentiation by both immunohistochemistry and electron microscopy. A prominent early theory held that renal MRTs were neuroectodermal in origin (20). Support for this theory comes from evidence of hormonal activity (21) and the observation of a greater than expected association between renal MRTs and primitive neuroectodermal tumors of the central nervous system (22, 23). This theory might explain the intraventricular location of two of our tumors, given the central location of the primordial neurons.

When MRT is diagnosed in the brain, an occult renal primary must be considered. In our three cases, abdominal CT scans demonstrated normal kidneys. Given the relentlessly progressive course of these tumors, it is highly unlikely that renal

MRT or other intraabdominal primaries would be clinically undetected.

The mean age of our patients (2.7 years) was similar to that of previously documented primary MRTs of the brain (2–7) listed in Tables 1 and 2. Two of our patients were female, whereas five of six previous cases have been in males. All of our patients had left cerebral tumors; locations in the previous cases were left cerebral (2, 3), posterior fossa (4–6), and multifocal (7). Two tumors in our series were intraventricular, whereas two of the four previous cases with sufficient surgical data (3, 6) indicated ventricular invasion. Serial postsurgical imaging in our patients revealed not only relapse at the primary site but also the development of rapidly growing meningeal masses consistent with leptomeningeal metastases. The latter finding was present in two of the previously reported cases (3, 5) and was likely responsible for the initial multifocal presentation of the tumor in another (7).

Our patients had a mean survival of 9 months from the time of surgery. The previous cases had even poorer outcome (median survival, 2.5 months). This discrepancy could reflect the aggressive postsurgical therapy used in our patients, including irradiation of the primary site. Of the six previous cases, one died prior to treatment (5) and one had surgery alone (3); only three patients had received chemotherapy and/or irradiation following surgery (2, 6, 7). No treatment information was reported for the remaining patient (4).

Although the preoperative imaging findings described here are nonspecific, there was some consistency among the three cases. All tumors were large and had multiple necrotic/cystic foci 1.0 to 2.5 cm in diameter. Two tumors had a patchy pattern of enhancement on CT and MR and were associated with moderate to marked adjacent parenchymal edema consistent with the aggressive nature of the tumor. The fact that two tumors in our series were located within the lateral ventricle suggests consideration of primary MRT in the differential diagnosis of large childhood lateral ventricular masses, which includes choroid plexus papilloma/carcinoma, primitive neuroectodermal tumor, and teratoma (24). The presence of enlarged ventricles and cisterns that are not mechanically obstructed by the tumor may favor choroid plexus papilloma, but the remaining diagnoses have CT findings similar to those seen with MRT.

In case number 3 in our series, no specific MR features were demonstrated. Although the T1- and T2-weighted signal characteristics of the solid tumor component were similar to those most commonly encountered with meningioma (25, 26), the enhancement pattern was distinctly different. Histologically, the T1- and T2-weighted tumor isointensity with gray matter was found to reflect prominent tumor cellularity characterized by diffuse sheets of round-to-oval tumor cells.

In summary, MRT of the brain is a rare, rapidly fatal primary brain tumor that should be considered in the differential diagnosis of large childhood intracranial neoplasms. The imaging findings in our series, although nonspecific, reflect the aggressive nature of the tumor. The striking tendency of this tumor to relapse and spread via the leptomeninges indicates the need for contrast-enhanced MR in the initial and serial assessments of disease extent.

Acknowledgments

We are grateful to Drs Tom Callihan and Olga Lassiter for loaning us the paraffin blocks on cases 1 and 2, to Hallie Holt for the immunohistochemical stains, and to Alice Slusher and Vicki Denison for electron microscopy assistance.

References

1. Beckwith JB, Palmer NF. Histopathology and prognosis of Wilms' tumor: results from the First National Wilms' Tumor Study. *Cancer* 1978;41:1937–1948
2. Sotelo-Avila C, Gonzalez-Crussi F, deMello D, et al. Renal and extrarenal rhabdoid tumors in children: a clinicopathologic study of 14 patients. *Semin Diagn Pathol* 1986;3:151–163
3. Briner J, Bannwart F, Kleihues P, et al. Malignant small cell tumor of the brain with intermediate filaments: a case of a primary cerebral rhabdoid tumor. *Pediatr Pathol* 1985;3:117–118
4. Kapur S, Patterson K. Primary rhabdoid tumor of the cerebellum. *Pediatr Pathol* 1986;5:110
5. Biggs PJ, Garen PD, Powers JM, Garvin AJ. Malignant rhabdoid tumor of the central nervous system. *Hum Pathol* 1987;18:332–337
6. Jakate SM, Marsden HB, Ingram L. Primary rhabdoid tumor of the brain. *Virchows Arch (A)* 1988;412:393–397
7. Ho PSP, Lee W-H, Chen C-Y, et al. Primary malignant rhabdoid tumor of the brain: CT characteristics. *J Comput Assist Tomogr* 1990;14:461–463
8. Weeks DA, Beckwith JB, Mierau GW, Luckey DW. Rhabdoid tumor of kidney: a report of 111 cases from the National Wilms' Tumor Study Pathology Center. *Am J Surg Pathol* 1989;13:439–458
9. Lynch HT, Shurin SB, Dahms BB, Izant RJ Jr, Lynch J, Danes BS. Paravertebral malignant rhabdoid tumor in infancy: in vitro studies of a familial tumor. *Cancer* 1983;52:290–296
10. Gonzalez-Crussi F, Goldschmidt RA, Hsueh W, Trujillo YP. Infantile sarcoma with intracytoplasmic filamentous inclusions: distinctive tumor of possible histiocytic origin. *Cancer* 1982;49:2365–2375
11. Small EJ, Gordon GJ, Dahms BB. Malignant rhabdoid tumor of the heart in an infant. *Cancer* 1985;55:2850–2853

12. Parham DM, Peiper SC, Robicheaux G, Ribeiro RC, Douglass EC. Malignant rhabdoid tumor of the liver: evidence for epithelial differentiation. *Arch Pathol Lab Med* 1988;112:61–64
13. Frierson HF Jr, Mills SE, Innes DJ Jr. Malignant rhabdoid tumor of the pelvis. *Cancer* 1985;55:1963–1967
14. Cho KR, Rosenshein NB, Epstein JI. Malignant rhabdoid tumor of the uterus. *Int J Gynecol Pathol* 1989;8:381–387
15. Perrone T, Swanson PE, Twiggs L, Ulbright TM, Dehner LP. Malignant rhabdoid tumor of the vulva: is distinction from epithelioid sarcoma possible? A pathologic and immunohistochemical study. *Am J Surg Pathol* 1989;13:848–858
16. Ekfors TO, Aho HJ, Kekomäki M. Malignant rhabdoid tumor of the prostatic region: immunohistological and ultrastructural evidence of epithelial origin. *Virchows Arch (A)* 1985;406:381–388
17. Tsuneyoshi M, Daimaru Y, Hashimoto H, Enjoji M. Malignant soft-tissue neoplasms with the histologic features of renal rhabdoid tumors: an ultrastructural and immunohistochemical study. *Hum Pathol* 1985;16:1235–1242
18. Rutledge J, Beckwith JB, Benjamin D, Haas JE. Absence of immunoperoxidase staining for myoglobin in the malignant rhabdoid tumor of the kidney. *Pediatr Pathol* 1983;1:93–98
19. Vogel AM, Gown AM, Caughlan J, Haas JE, Beckwith JB. Rhabdoid tumors of the kidney contain mesenchymal specific and epithelial specific intermediate filament proteins. *Lab Invest* 1984;50:232–238
20. Haas JE, Palmer NF, Weinberg AG, Beckwith JB. Ultrastructure of malignant rhabdoid tumor of the kidney: a distinctive renal tumor of children. *Hum Pathol* 1981;12:646–657
21. Mayes LC, Kasselberg AG, Roloff JS, Lukens JN. Hypercalcemia associated with immunoreactive parathyroid hormone in a malignant rhabdoid tumor of the kidney (rhabdoid Wilm' tumor). *Cancer* 1984; 54:882–884
22. Bonnin JM, Rubinstein LJ, Palmer NF, Beckwith JB. The association of embryonal tumors originating in the kidney and in the brain: a report of seven cases. *Cancer* 1984;54:2137–2146
23. Howat AJ, Gonzales MF, Waters KD, Campbell PE. Primitive neuroectodermal tumor of the central nervous system associated with malignant rhabdoid tumor of the kidney: report of a case. *Histopathology* 1986;10:643–650
24. Jelinek J, Smirniotopoulos JG, Parisi JE, Kanzer M. Lateral ventricular neoplasms of the brain: differential diagnosis based on clinical, CT, and MR findings. *AJNR* 1990;11:567–574
25. Zimmerman RD, Fleming CA, Saint-Louis LA, Lee BCP, Manning JJ, Deck MDF. Magnetic resonance imaging of meningiomas. *AJNR* 1985;6:149–157
26. Elster AD, Challa VR, Gilbert TH, Richardson DN, Contento JC. Meningiomas: MR and histopathologic features. *Radiology* 1989; 170:857–862